WMM20 conference

November 3rd to 5th,2020 - Rome, Italy

Electrical Steel and Motors performances, Role of Lamination Thickness

Mircea Popescu and Nicolas Riviere
Motor Design Ltd.
5 Edison Court, Wrexham
Wales, UK

Summary

The electrical machines main component is represented by the magnetic cores. These are manufactured using mostly laminated electrical steels. The properties of the electrical steel: magnetic permeability, maximum flux-density, specific losses are determining the machines performance. This study compares the performance of newly developed induction motors for traction application in electrical vehicles, by considering four types of laminated electrical steel grades. The analysis shows the impact of magnetization curves and losses on the motors' outputs.

1 Introduction

1.1 Electrical Steel Consideration

The specific materials suitable for electric motor design in traction applications, include electrical steels and copper alloys. Considering the rotational speed, it is possible to select optimum materials for the electric motor from the mechanical point of view.

For the stator and rotor laminations, different silicon–iron (SiFe) and cobalt–iron (CoFe) alloys can be considered. CoFe ensures highest saturation magnetization, going above 2 Tesla, thus enabling highest power densities to be achieved. The actual value of saturation magnetization for CoFe depends on the annealing temperature, time of annealing, and annealing atmosphere; in general, the better the mechanical characteristics of the annealed material, the lower the saturation magnetization. However, even when annealed to the optimum mechanical properties, the saturation magnetization of CoFe is still significantly higher than SiFe (around 20% higher). Materials of CoFe type, are significantly more expensive compared with SiFe laminations, hence the material weight per kilowatt is intrinsically higher and is thus not considered for this project.

Another important parameter when choosing the lamination material for electric motor is the amount of core losses generated in the lamination due to the relatively high fundamental (up to 1kHz) and switching frequencies (up to 20kHz). For a given frequency and flux density, the core losses are primarily influenced by the lamination thickness and the final annealing method. In general, the thinner the laminations, the lower the core losses. Electrical steels as thin as 0.1 mm with very low core losses, which are tailored specifically for high-frequency applications, are commercially available but again too expensive to electric motor in EVs.

Figure 1 compares the mechanical yield-strength and core-loss characteristics for commercially available steel grades. Square symbol denotes CoFe steel type, and diamond symbol denotes SiFe steel type. M270-35A and M235-35A are common 0.35-mm thickness SiFe grades with a typical yield strength of around 350MPa and 450MPa, respectively. These grades are typically used for higher performance volume-manufactured mainstream motors such as traction machines. A cost-effective alternative is also SiFe thinner grades than 0.35mm, such as NO30 and NO20, which have 0.30mm and 0.20mm respectively thickness. The core losses are lower, but the cost is higher, and the yield stress is typically reduced.

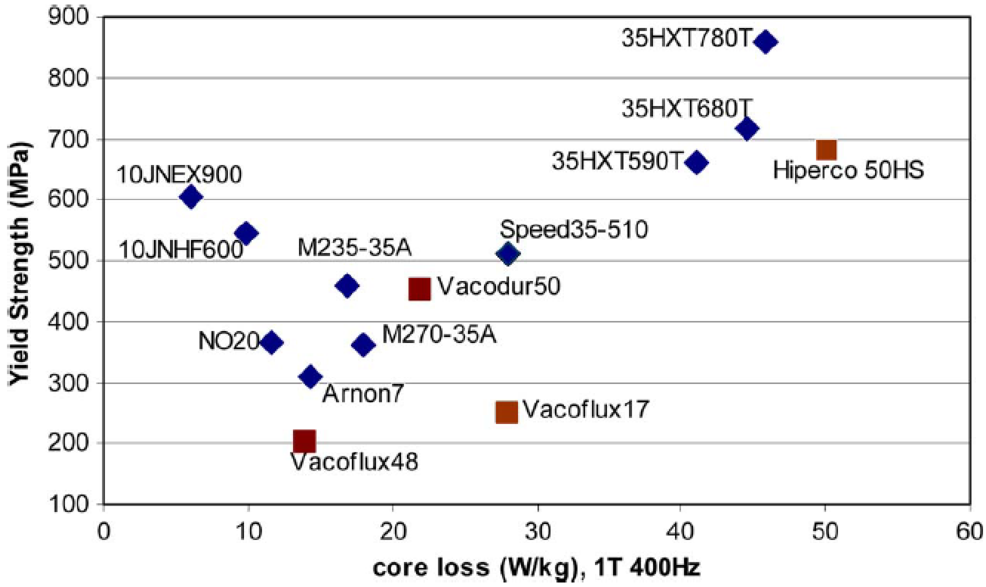

Figure 1 Comparison of core losses and yield strength for different high performance electrical steels [1]

2 Induction Machine Case

2.1 Specifications

The Electrical Vehicles' (EVs) market has kept growing for the last decade, due to new environmental restrictions made by governments to reduce gas emissions and to prepare the ecological transition towards the fossil fuel independency. Compared to conventional combustion engines, the electric motors benefit of higher efficiency, braking recovery and provides a noise free solution with a smoother driving, bettering passengers, and pedestrians comfort. To limit the global energy consumption and ensure a modular integration into the vehicle, the market demand tends towards more efficient, lighter, and more compact motors.

The present study focuses on the development of next generation electric powertrain, avoiding the use of magnets and ensuring the industrial feasibility for mass production at low manufacturing costs. The Induction Machine (IM) is therefore considered a potential candidate. The specifications are reported in TABLE I. The Key Performance Indicators (KPIs), including efficiency, specific torque, specific power and power density are defined based on Tesla 60s motor [1]. Additional boundary conditions are set based on vehicle requirements, considering the Jaguar XJMY21 as a target.

TABLE I. MOTOR SPECIFICATIONS

Requirement	Unit	Value
Peak power	kW	200
Peak torque	Nm	371
Maximum speed	rpm	22000
Nominal torque	Nm	152
Nominal power	kW	70
Peak specific power	kW/kg	4.3*
Peak specific torque	Nm/kg	8.2*
Peak power density	kW/l	8*
Efficiency	%	$\geq$ 94
Maximum DC bus voltage	V	720
Maximum phase current	Arms	500

Maximum dimensions	mm	250 × 250 X 310

2.2 Machine topology

Even if induction machines present a lower efficiency and torque density than PM motors, the technology is well established in the automotive industry (e.g. Tesla Motors) and it still represents an attractive and feasible solution for EVs, due to its simplicity, robustness, versatility, cost-effective manufacturing aspects and fault tolerant capability. In addition, the IM does not use rare-earth materials, ensuring mass production feasibility at lower cost [3]. The copper is usually preferred to the aluminium due to its higher electrical conductivity, higher mechanical strength and better thermal properties. The rotor can be either die-casted or fabricated and both methods are now industry proven [4].

A hairpin winding is used on the stator side. The proposed designs for the IM use exceptional performance of the proprietary hairpin stator winding**.** In contrast to conventional round wire windings, the hairpin stator winding uses precision-formed rectangular wires. Multiple layers of interlocking “hairpins” produce a superior slot fill (up to 73% vs. 40% for typical round-wire windings) [5], [8]. From a thermal perspective, the machine will be stator and rotor cooled and two different solutions are investigated. The first one consists of conventional housing water jacket coupled with a spiral groove shaft cooling system, using a mixture of ethylene, water and glycol mixture as a coolant. The second one is equipped with a spray cooling system with nozzles places on the housing jacket and the hollow shaft surface, cooled by automatic transmission fluid.

The adopted designs are outlined in Figure 2. A copper rotor induction motor (CR-IM) topology is employed: stator with 36 slots and rotor with 50 bars topology are used for

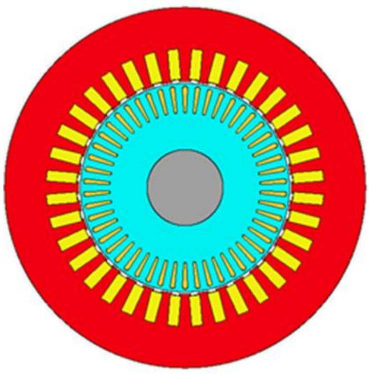

(a)

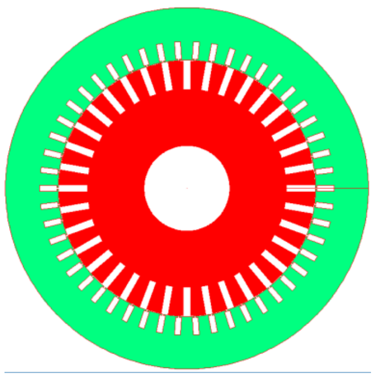

(b)

Figure 2 Radial and axial cross sections of proposed induction motor designs: a) inner rotor; b) outer rotor

both (a) inner and (b) outer rotor configurations. The number of magnetic poles is different for two configurations: 4-pole for inner rotor, and 6-pole for outer rotor respectively. The active weight and dimensions are within the limits specified in section **Errore. L'origine riferimento non è stata trovata.** and the main characteristics will be provided in full paper version.

3 Material Selection

3.1 Types of Electrical Steel

Four non-oriented electrical steel, silicon-iron type, have been considered for CR-IM. Tests on the steel samples have been performed by RINA-CSM [2]:

- Material 1: M235-35A (Non-Oriented, fully-processed, thickness 0.35 mm)
- Material 2: M290-50JKE (Non-Oriented, semi-processed, thickness 0.50 mm)
- Material 3: NO30-15 (Non-Oriented, fully-processed, thickness 0.30 mm)
- Material 4: NO02-HS (Non-Oriented, fully-processed, thickness 0.20 mm)
- Frequencies used in tests: 50Hz, 400Hz, 800Hz, 1000Hz
- Induction up to 1.6T; extrapolated by MDL to 2.1T in modelling CR-IM.

All materials were laser cut and with a comparison of the measured data summarized in Figures 3 and 4.

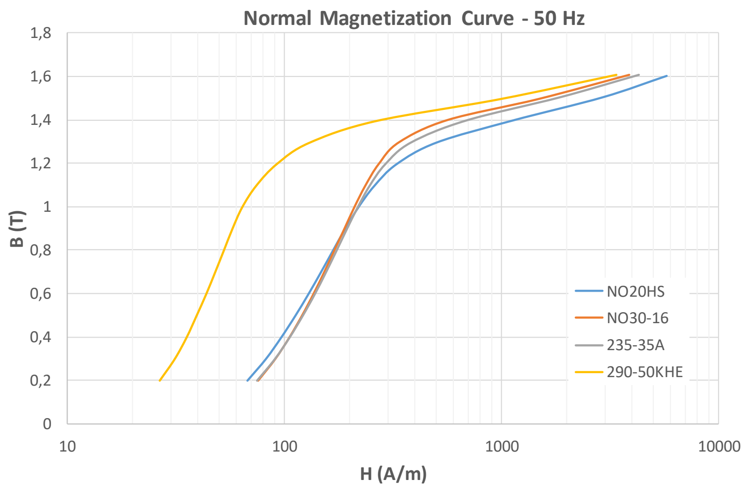

Figure 3 Magnetizing curve at 50 Hz

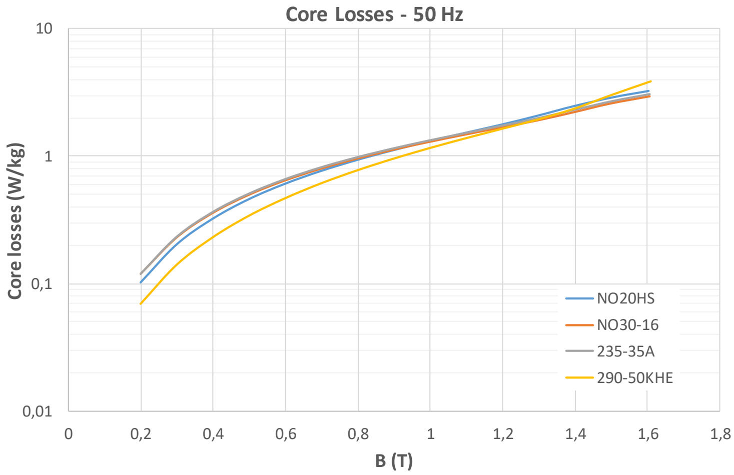

Figure 4 Specific core losses at 50Hz

The analysis performed for the designs in section 2.2, for inner CR-IM and outer CR-IM lead to the following conclusions:

- BH curve values effect:
    - 50Hz would estimate 370Nm peak torque vs 400Hz would estimate 350Nm; small drop in magnetizing current.
- Inner CR-IM:
    - Very little impact on performance, as most of losses are in stator winding and copper cage.
    - <u>Best choice will be M235-35A</u> considering cost/performance ratio.
- Outer CR-IM:
    - With NO20 and NO30, can reach 95% efficiency in a small area
    - M290-50JKE is clearly leading to poorer performance.
- Best choice will be M235-35A considering cost/performance ratio.

The frequency values used in tests are: 50Hz, 400Hz, 800Hz, 1000Hz and induction levels were up to 1.8T; extrapolated to 2.1T in modelling.

3.2 Mechanical and Chemical Analysis

Mechanical characterizations were performed by RINA-CSM on the selected material M235-35A and NO30-15. Figure 5 shows one of the tested specimens under tensile conditions.

Figure 5. Electrical steel specimen after a tensile test

Errore. L'origine riferimento non è stata trovata.7 represent the stress-strain characteristics obtained in the transverse and longitudinal directions for two specimens of different lengths (L-1, L-2). The parts of the curves of interest, that is the linear parts, are very close to each other, leading to similar mechanical properties in the two considered directions, as presented in Tables IV and V. Also note that the measurements are in line with catalogue data.

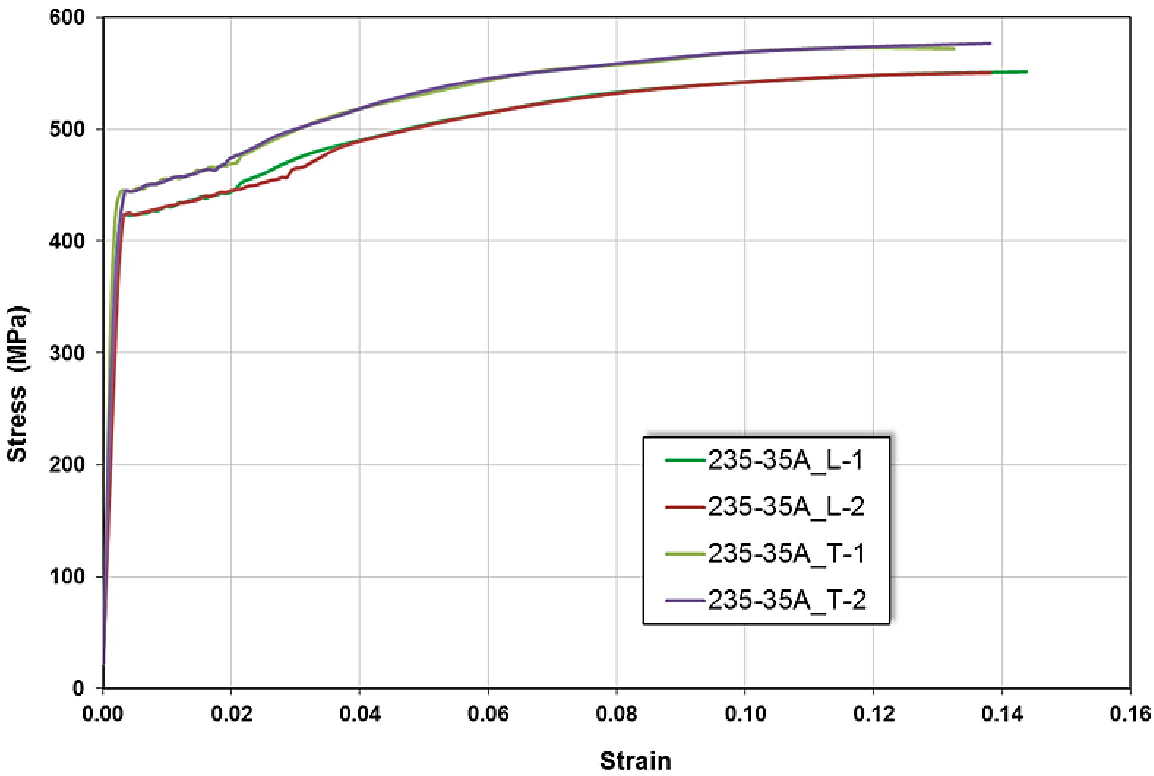

Figure 6 Measured stress-strain characteristics (M235-35A)

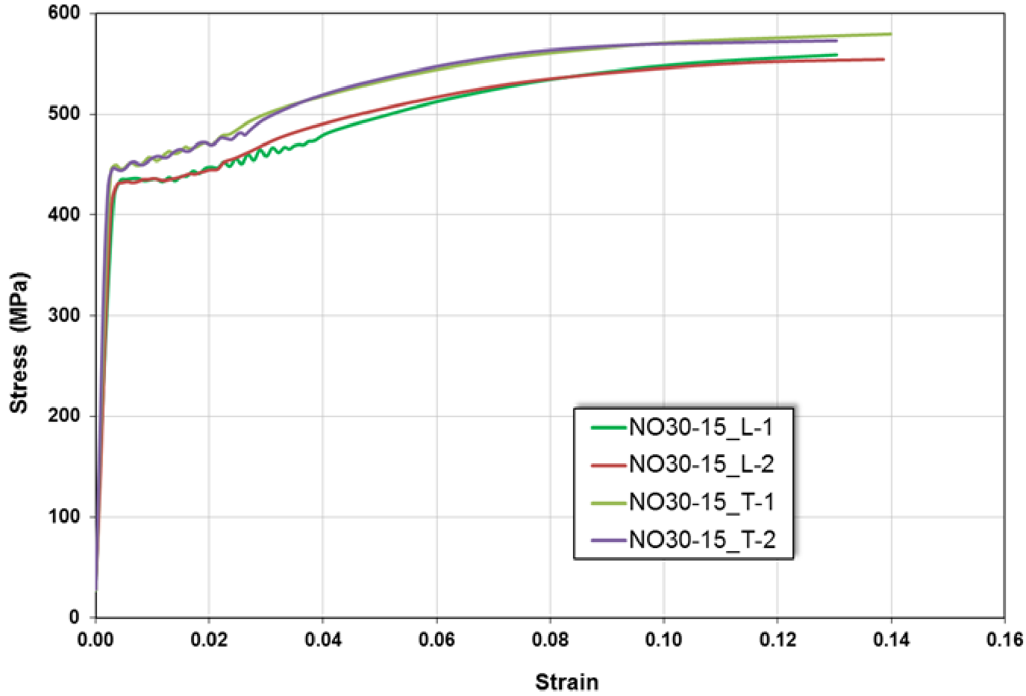

Figure 7 Measured stress-strain characteristics (NO30)

Table IV. Mechanical properties calculated from tensile tests (M235-35A and NO30)

Material	**Specified Values**			**Experimental Values**			
	Yield strength R_{p02} [MPa]	Ultimate strength R_m [MPa]	Elongation A_{80} [%]	Yield strength R_{p02} [MPa]	Ultimate strength R_m [MPa]	Elongation A_{50} [%]	Specimen orientation
NO30-15	-	-	-	446-444	580-573	18.9-15.7	TRASV
	430	540	18	435-433	559-554	22.1-20.8	LONG
M235-35A	430	550	18	444-444	572-577	23.6-22.7	TRASV
	-	-	-	423-424	551-550	20.5-21.6	LONG

Table V. Chemical properties calculated from tensile tests (M235-35A and NO30)

Material	Type	Nominal Density (g/cm^2)	Resistivity (Ω·m)	C (ppm)	Si (%)	Al (%)	Mn (%)	Cu (%)	S (ppm)	N (ppm)	Ti (ppm)
M235-35A	NGO	7,60	62,91 (*)	56	2,60	1,43	0,50	0,013	18	18	52
NO30-15	NGO	7,60	61,14 (*)	67	2,57	1,37	0,54	0,013	16	15	45

3.3 Electromagnetic Analysis

Figure **2**8 to Figure **9**14 show the estimated efficiency for IR-IM and OR-IM designs considering all four non-oriented electrical steel materials. It is observable that except for material grade M290-50JKE, the other three grades lead to practically similar results:

- Maximum magnetizing current level shows a similar overall magnetic permeability of the considered electrical steel; this is explicable by the fact that the motor is highly saturated at peak supply current.
- Core losses represent just a minor fraction within the total losses; for the proposed designs, total losses are dominated by the Joule loss components, in stator winding and rotor cage.

Errore. L'origine riferimento non è stata trovata.VI and **Errore. L'origine riferimento non è stata trovata.**VII summarize the CR-IM parameters that are affected by the electrical steel grade for both topologies.

TABLE VI CR-IM INNER ROTOR PERFORMANCE WITH VARIOUS ELECTRICAL STEEL GRADES

Property	**Unit**	**M235-35A**	**M290-50JKE**	**NO30-15**	**NO20-HS**
Magnetizing Current@50Hz	Arms	162	160	169	168
Magnetizing Current@400Hz	Arms	157	152	156	155
Maximum Torque@50Hz/400Hz	N.m	370/350	370/350	370/350	370/350
Maximum Core Loss/ Total Loss	W	980/31500	1600/31500	750/31500	840/31500

TABLE VII CR-IM OUTER ROTOR PERFORMANCE WITH VARIOUS ELECTRICAL STEEL GRADES

Property	**Unit**	**M235-35A**	**M290-50JKE**	**NO30-15**	**NO20-HS**
Magnetizing Current@50Hz	Arms	170	170	170	170
Magnetizing Current@400Hz	Arms	170	170	170	170
Maximum Torque@50Hz/400Hz	N.m	350/320	350/320	350/320	350/320
Maximum Core Loss/ Total Loss	W	3150/29000	7200/31500	2500/25000	2400/27000

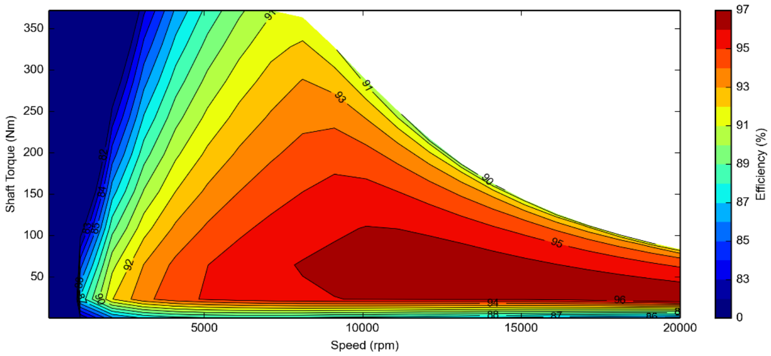

(a) Efficiency Map

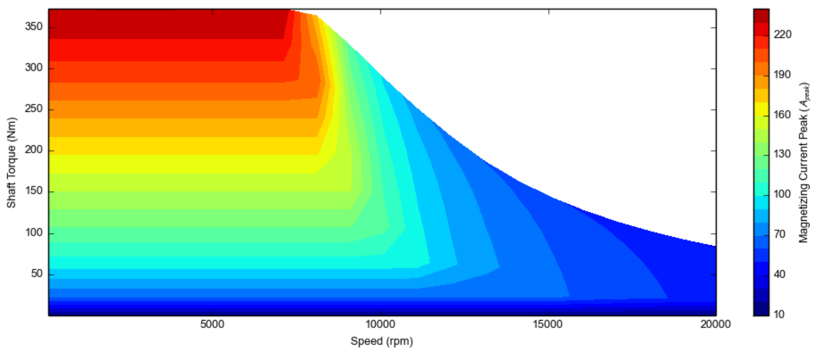

(b) Magnetizing current Map (max 230A)

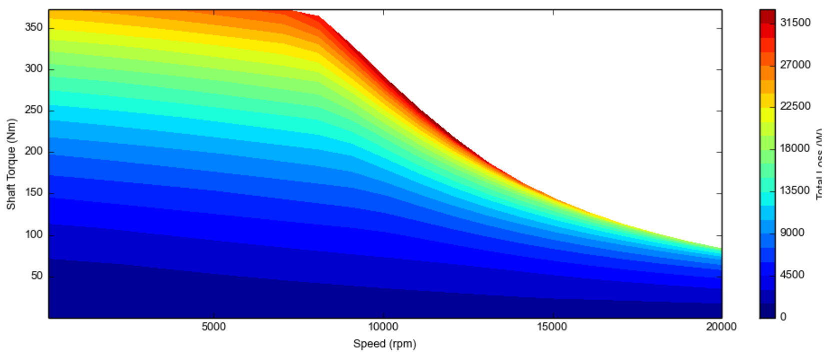

(c) Total Loss Map (max 31500W)

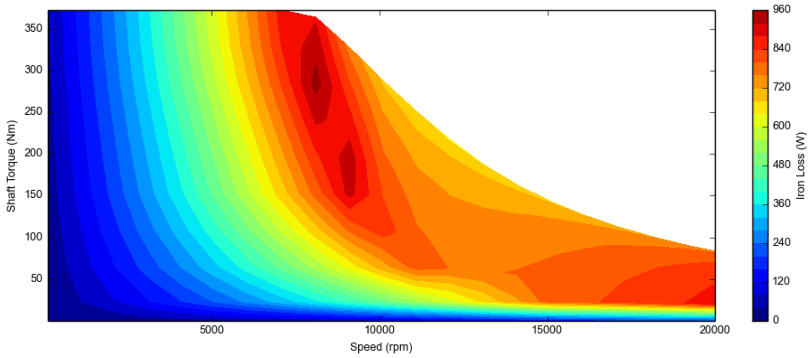

(c) Core loss Map (max 980W)

Figure 2. IR-IM performance with M235-35A electrical steel, BH curve at 50Hz

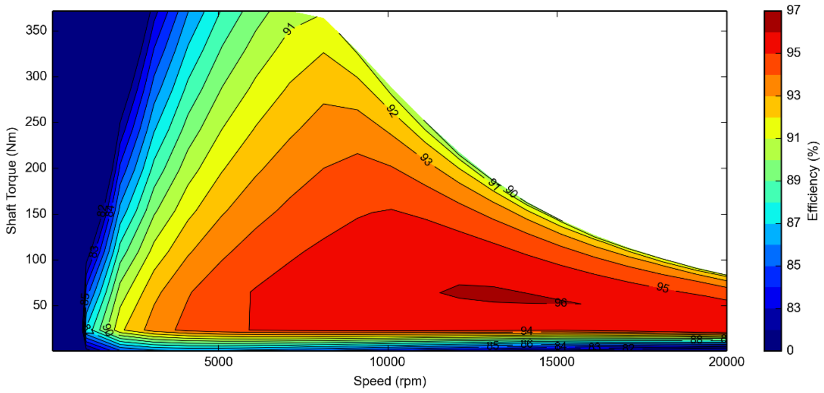

(a) Efficiency Map

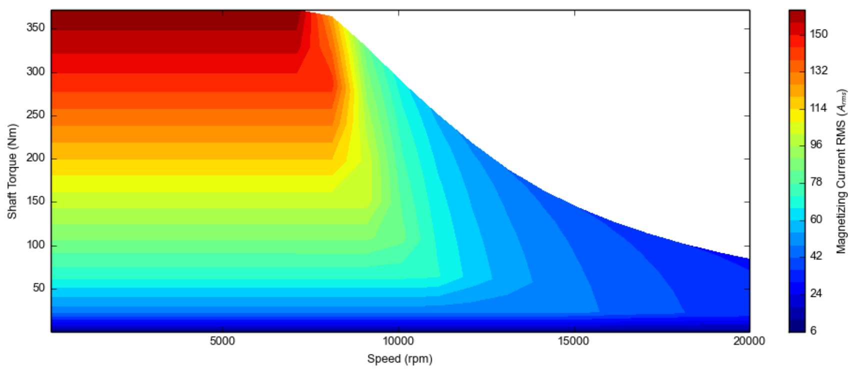

(b) Magnetizing current Map (160Arms/220A)

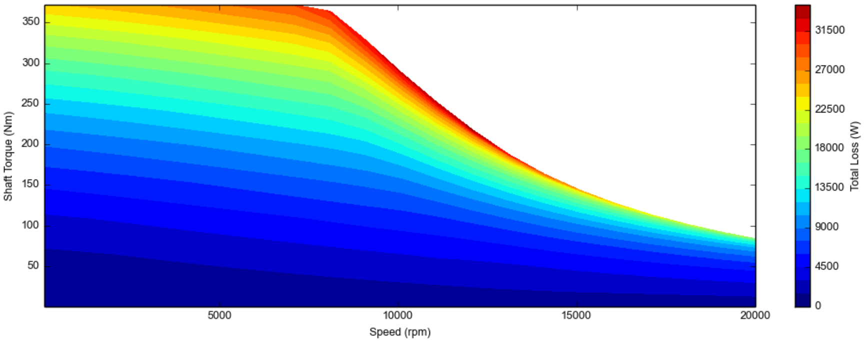

(c) Total loss Map (31500W)

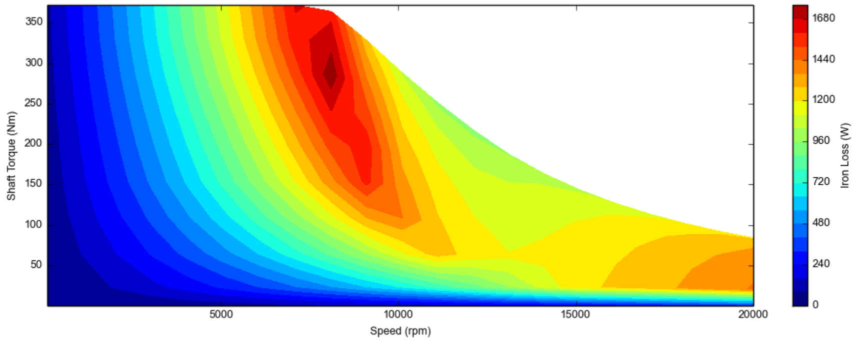

(d) Core Loss Map (max 1600W)

Figure 3. IR-IM performance with M290-50JKE electrical steel, BH curve at 50Hz

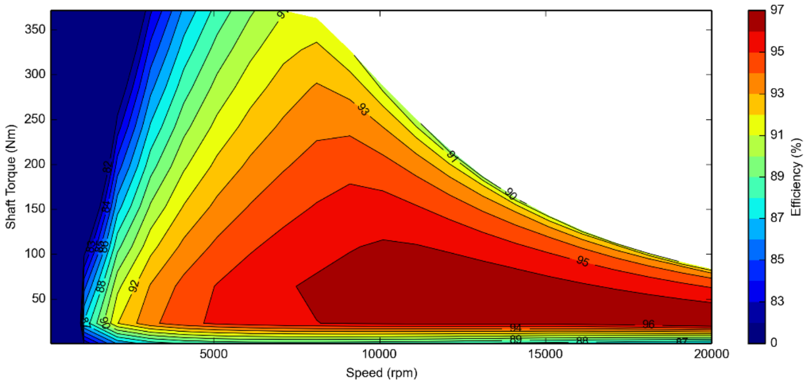

(a) Efficiency Map

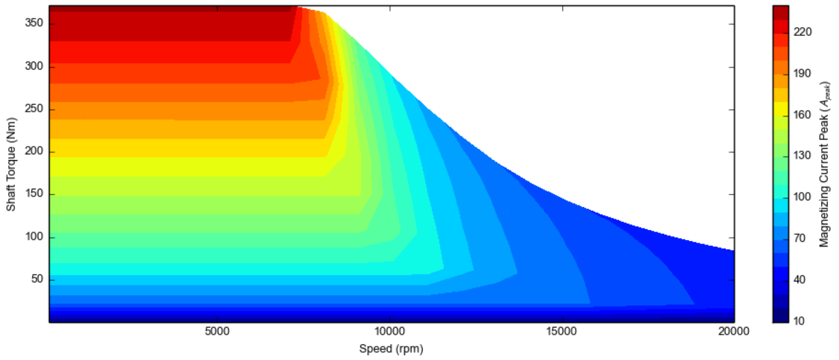

(b) Magnetizing current Map (220 A)

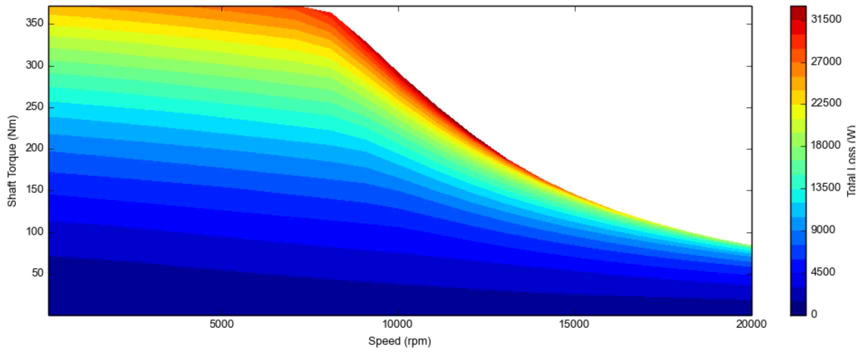

(c) Total loss Map (max 31500W)

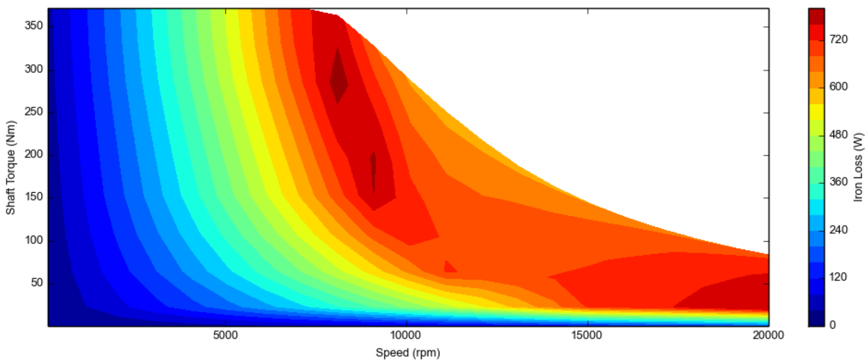

(d) Core loss Map (max. 750W)

Figure 4. IR-IM performance with NO30-15 electrical steel, BH curve at 50Hz

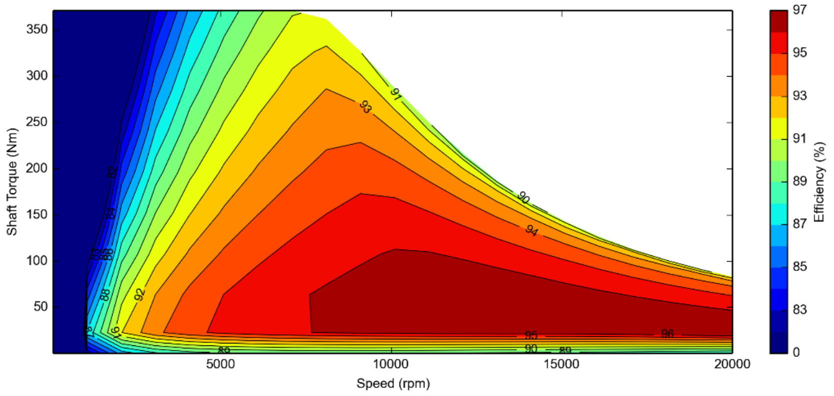

(a) Efficiency Map

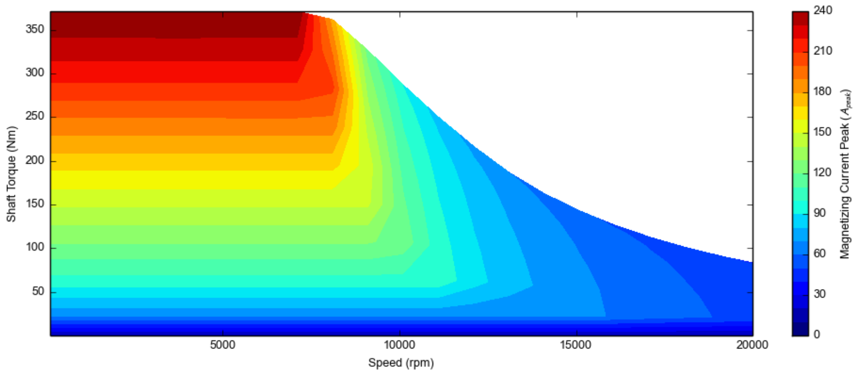

(b) Magnetizing current Map (max. 240A)

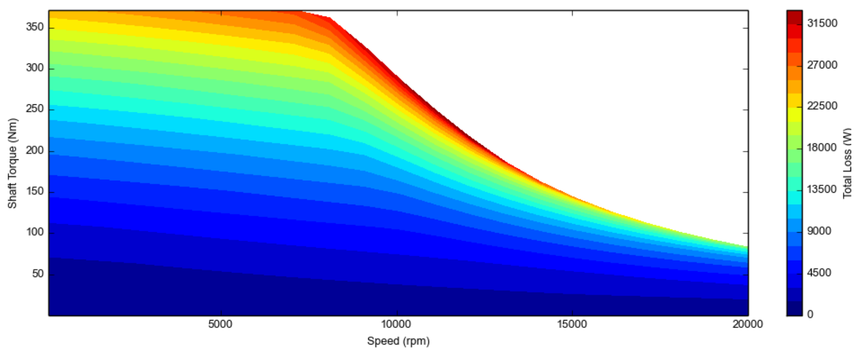

(c) Total losses Map (max 31500W)

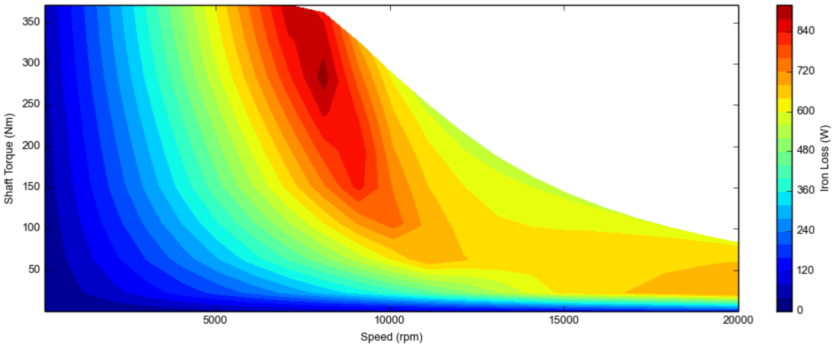

(d) Core loss Map (max. 840W)

Figure 5. IR-IM performance with NO20-HS electrical steel, BH curve at 50Hz

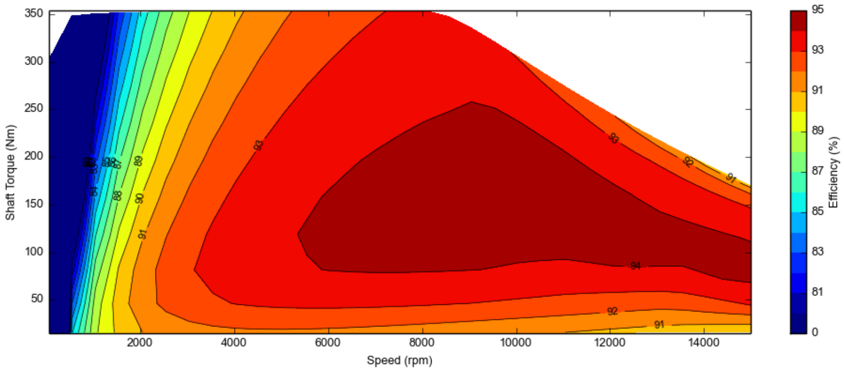

(a) Efficiency Map

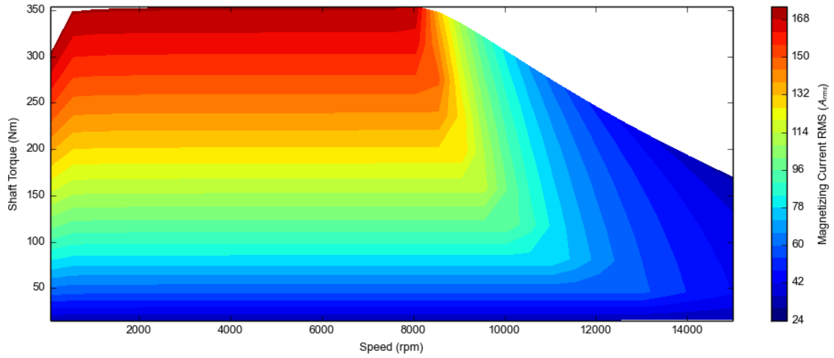

(b) Magnetizing current Map (max. 170Arms)

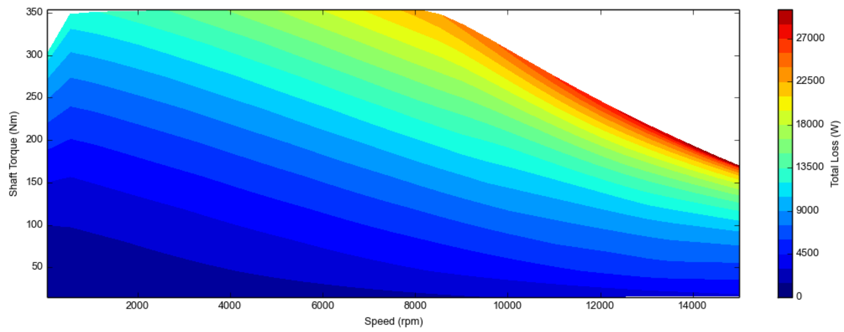

(c) Total losses Map (max. 29000W)

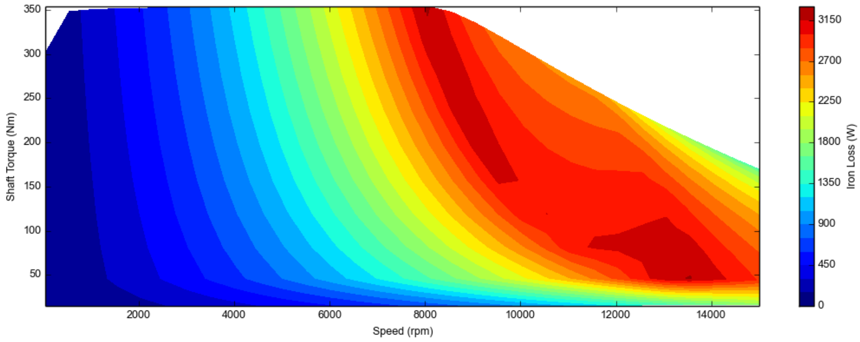

(d) Core losses Map (max. 3150W)

Figure 6. OR-IM performance with M235-35A electrical steel, BH curve at 50Hz

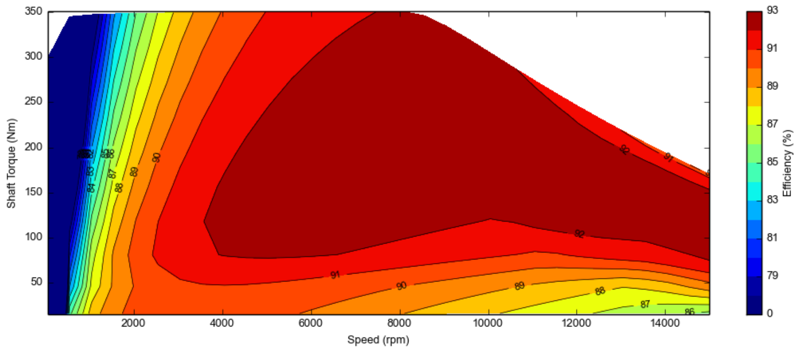

(a) Efficiency Map

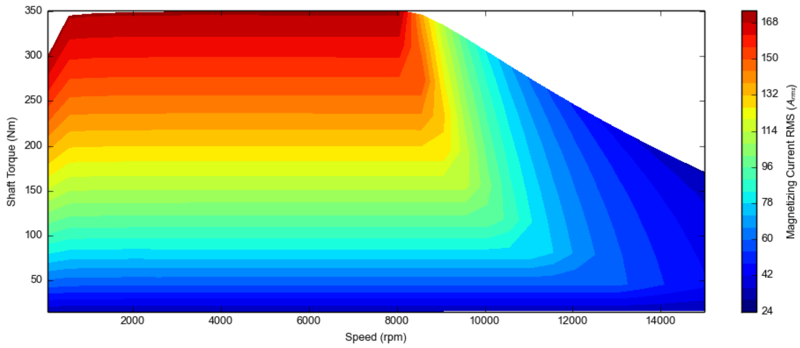

(b) Magnetizing current Map (max. 170Arms)

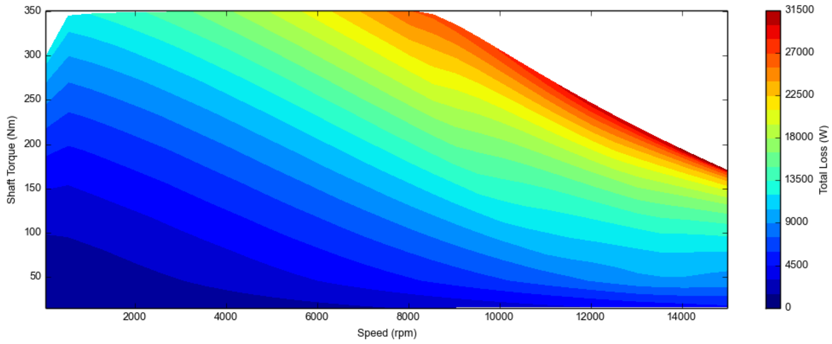

(c) Total losses Map (max. 31500W)

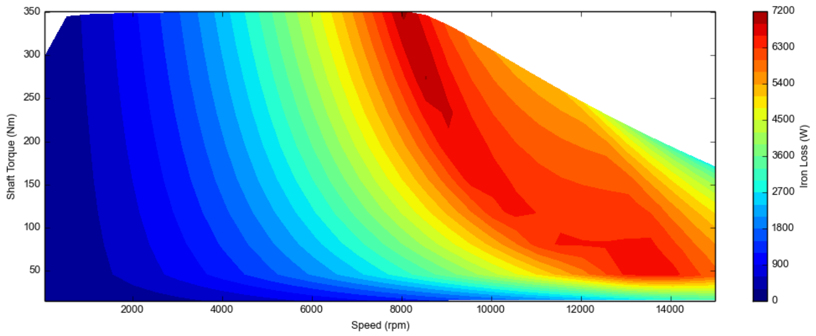

(d) Core losses Map (max. 7200W)

Figure 7. OR-IM performance with M290-50JKE electrical steel, BH curve at 50Hz

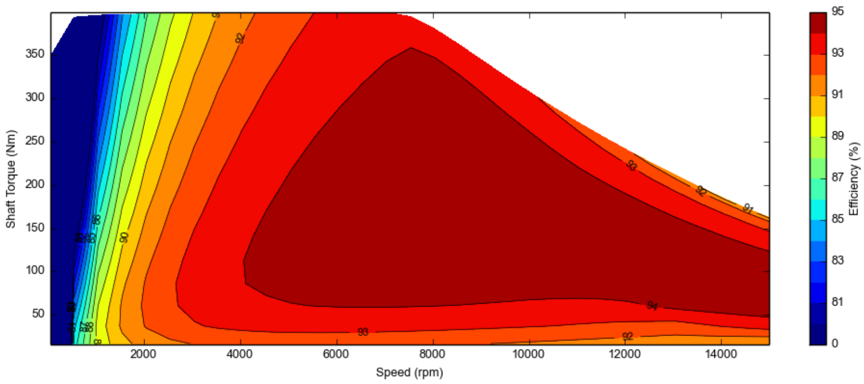

(a) Efficiency Map

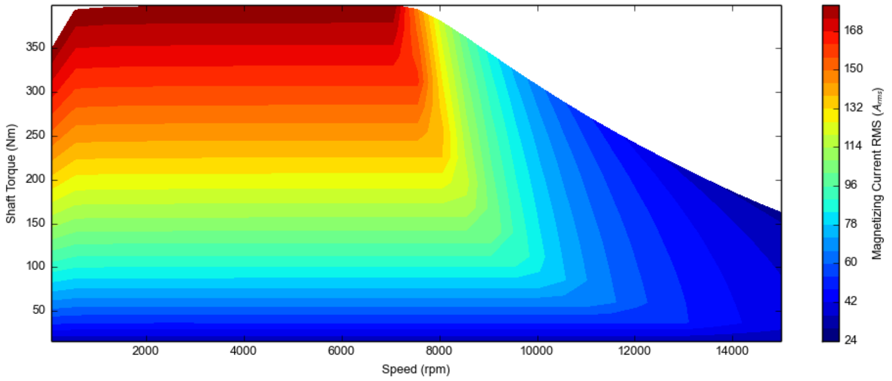

(b) Magnetizing current Map (max. 170Arms)

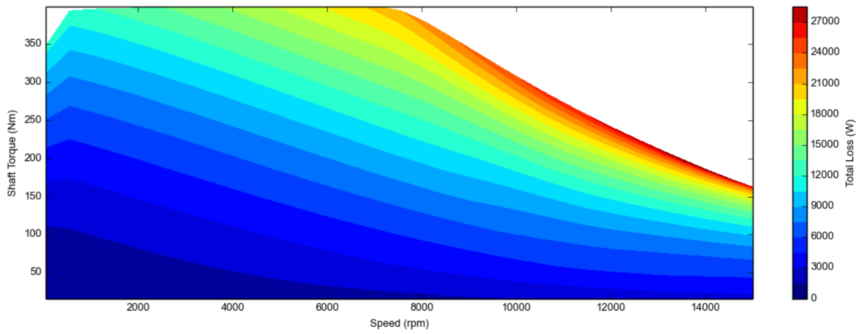

(c) Total losses Map (max. 27000W)

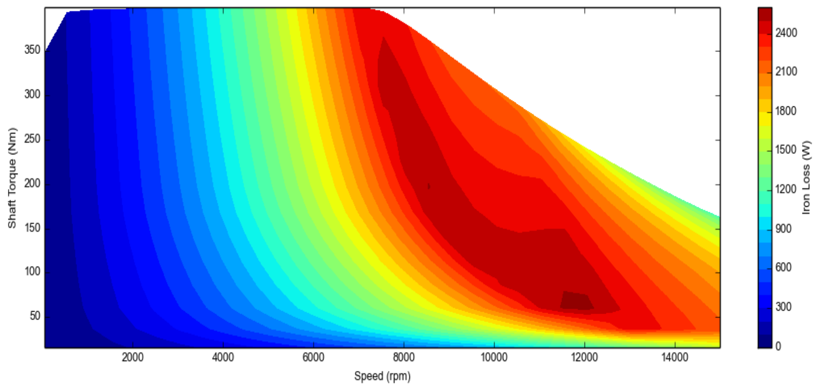

(d) Core losses Map (max. 2500W)

Figure 8. OR-IM performance with NO30-15 electrical steel, BH curve at 50Hz

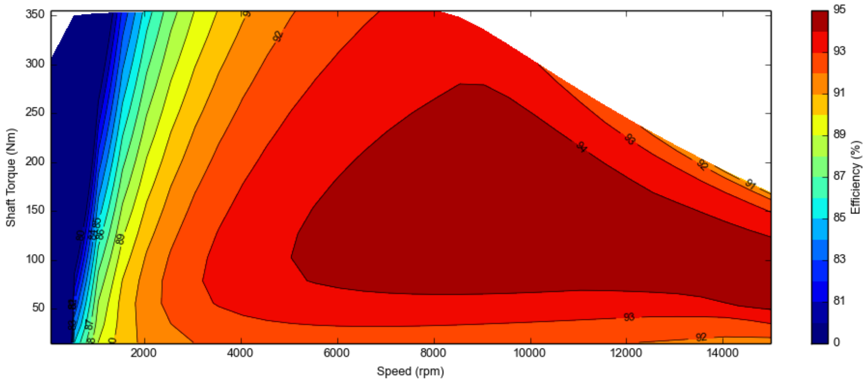

(a) Efficiency Map

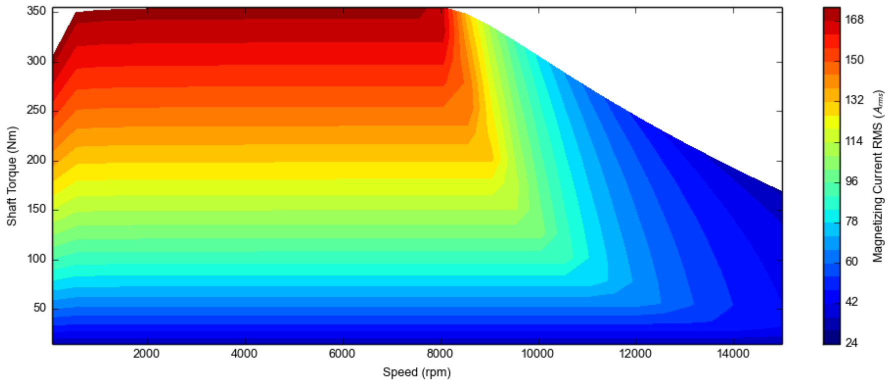

(a) Magnetizing current Map (max. 170Arms)

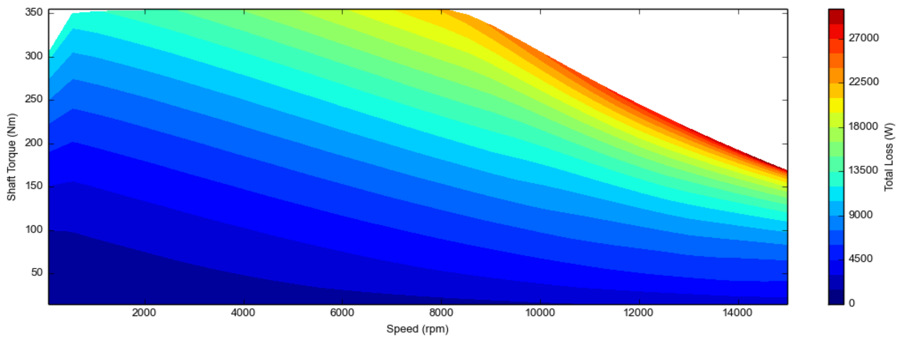

(a) Total losses Map (max. 27000W)

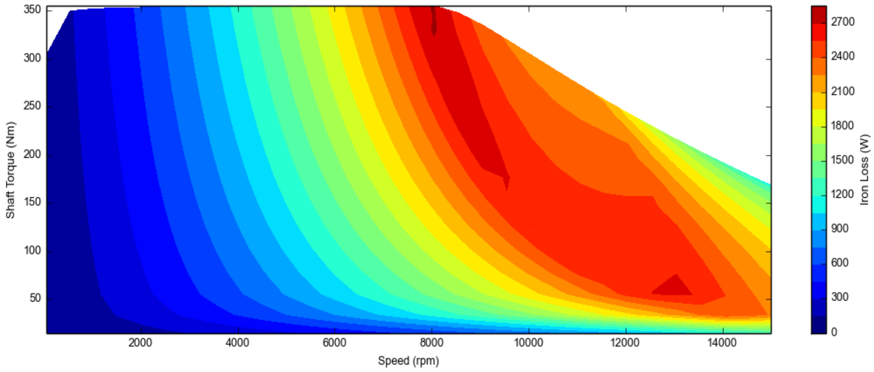

(a) Core losses Map (max. 2400W)

Figure 9. OR-IM performance with NO20-HS electrical steel, BH curve at 50Hz

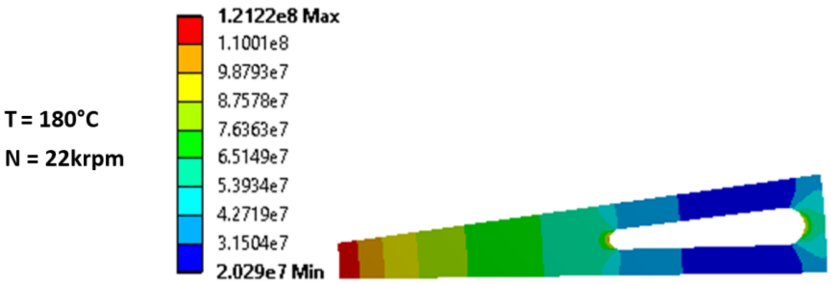

(a)

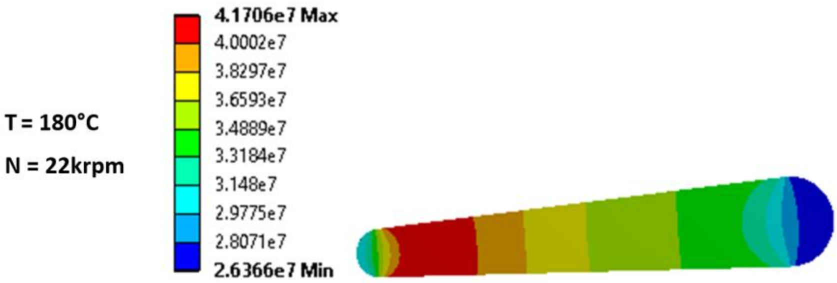

(b)

Figure 10. Von Mises stress for inner rotor CR-IM, with (a) rotor core M235-35A steel and (b) copper bar (units in Pa)

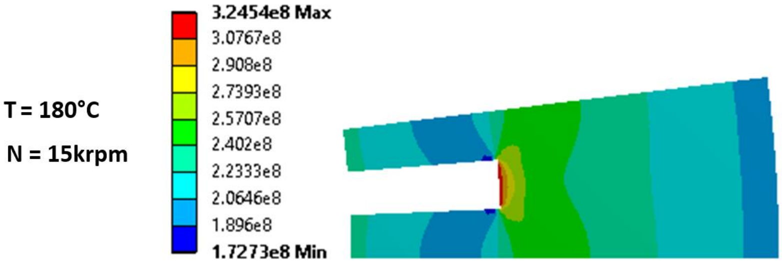

(a)

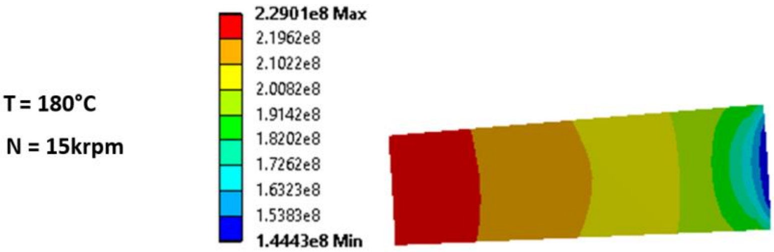

(b)

Figure 11 Von Mises stress for outer rotor CR-IM, with (a) rotor core M235-35A steel and (b) copper bar (units in Pa)

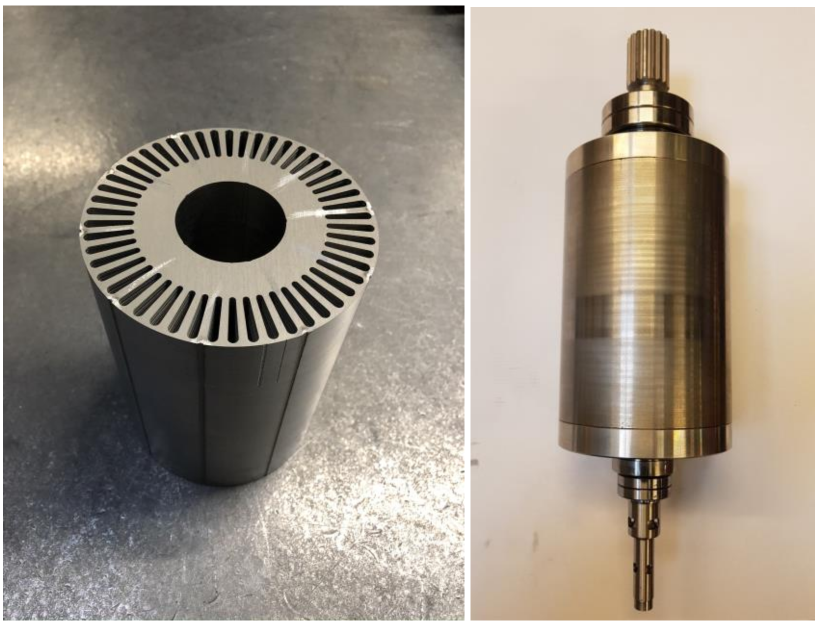

(a) Rotor Laminated Pack (b) Rotor Assembly

Figure 12. Rotor laminated pack and assembly using M235-35A

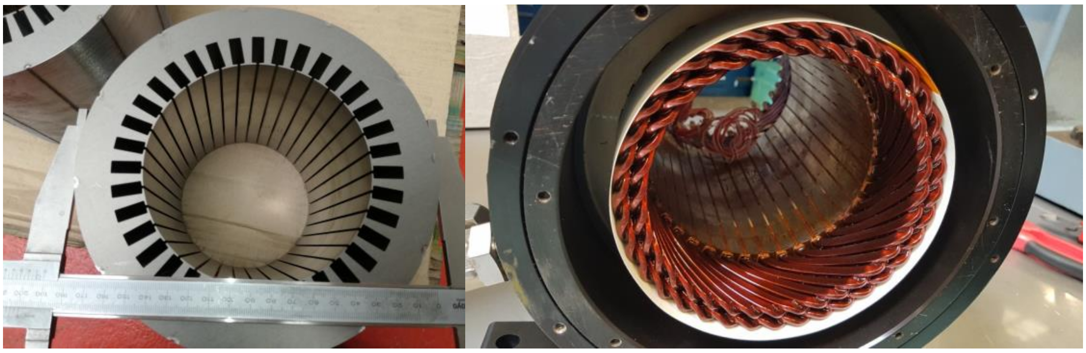

(a) Stator Laminated Pack (b) Stator Assembly

Figure 13. Rotor laminated pack and assembly using M235-35A

The results for mechanical stress analysis performed at maximum speed and temperature for inner and outer rotor topologies are given in Figures 16 and 17, respectively. Notice the limitations for outer rotor, where both the rotor lamination and rotor bar can be subjected to plastic deformation, i.e. Von Mises stress is close or higher than Yield stress. Therefore, the inner rotor configuration was selected for prototyping.

The laminated packs and assembly units for rotor and stator are shown in Figures 18 and 19, respectively.

4 Conclusion

The potential of induction machines in power traction systems for EV is investigated in this papers. The impact of the quality of electrical steel on the induction motor performance shows that induction machine for higher speed operation benefit mostly from higher magnetic permeability and to a certain extent from lower losses in the magnetic cores. However, due to the much higher loss component represented by winding and rotor cage losses, the contribution of core losses represents less than 5% of total losses in inner rotor configuration and 10-20% in outer rotor configuration.

Outer rotor configuration is limited due to mechanical stress values to lower speed (low gear ratio), when peak torque at low speed is the essential performance parameter. Inner rotor configuration represents a very good solution for higher speed, high power density solutions (high gear ratio).

For reference, the hairpin winding was the preferred technology for such application, due to the reduced DC copper loss and manufacturing suitable for automation. Copper cages can be built using two technologies, die-cast and fabricated, with similar performance.

As a final outcome of this study, the electrical steel grade is recommended to remain non-oriented, fully processed silicon iron, 0.35mm thickness, with possible grades: M235-35A, M250-35A, M270-35A or equivalent.

Acknowledgment

This work was funded under Horizon 2020, GV04 program, grant No. 770143.

The authors would like to acknowledge and thank their colleagues from RINA–Centro Sviluppo Materiali, Tecnomatic, Aurubis and Breuckmann for their contributions and useful discussions.

5 References

[1] . D. Gerada et al, *“High-speed electrical machines: Technologies, Trends and Developments”*, IEEE Transactions on Ind. Electronics., Vol. 61, No. 6, June 2014

[2] . https://www.rina.org/it

[3] . *Tesla Model S Pricing and Specs Revealed*, MotorWard, 2011 [Online]. Available : http ://www.motorward.com/2011/12/tesla-model-s-pricing-and-specs-revealed/

[4] . M. Burwell, J. Goss and M. Popescu “Performance/Cost Comparison of the Induction Motor and Permanent Magnet Motor in a Hybrid Electric Car” TechnoFrontier 2013, Tokyo, Japan

[5] . R. Tiwari, Dr. A.K. Bhardwaj, “*Analysis of Induction Motor with die-cast rotor*”. International Journal of Innovative Research in Electrical, Electronics, Instrumentation and Control Engineering, Vol 2, Issue 6

[6] . *Inside the HVH Hybrid Motor – Technical insights on Remy’s “Off-the-Shelf” Hybrid Motor Solutions*, White Paper, Remy Electric Motors, 2009

[7] . M. Caprio, V. Lelos, J. Herbst, S.Manifold, and H. Jordon, “*High strength induction machine, rotor, rotor cage end ring and bar joint, rotor end ring, and related methods*,” U.S. Patent 7 504 756, Mar. 17, 2009.

[8] . S. Jurkovic, K. Rahman, J. Morgante *”Induction Machine Design and Analysis for General Motors e-Assist Electrification Technology”,* IEEE Transactions on Ind. App., Vol. 51, No. 1, Jan/Feb 2015

[9] N. Riviére, M. Villani and M. Popescu, "Optimisation of a High Speed Copper Rotor Induction Motor for a Traction Application," IECON 2019 - 45th Annual Conference of the IEEE Industrial Electronics Society, Lisbon, Portugal, 2019, pp. 2720-2725, doi: 10.1109/IECON.2019.8927627.

[10] M. Popescu, N. Riviere, G. Volpe, M. Villani, G. Fabri and L. di Leonardo, "A Copper Rotor Induction Motor Solution for Electrical Vehicles Traction System," 2019 IEEE Energy Conversion Congress and Exposition (ECCE), Baltimore, MD, USA, 2019, pp. 3924-3930, doi: 10.1109/ECCE.2019.8912248.

[11] L. Di Leonardo, M. Popescu, M. Tursini and M. Villani, "Finite Elements Model Co-Simulation of an Induction Motor Drive for Traction Application," IECON

2019 - 45th Annual Conference of the IEEE Industrial Electronics Society, Lisbon, Portugal, 2019, pp. 1059-1065, doi: 10.1109/IECON.2019.8926853.

[12] L. di Leonardo, M. Popescu, G. Fabri and M. Tursini, "Performance Evaluation of an Induction Motor Drive for Traction Application," IECON 2019 - 45th Annual Conference of the IEEE Industrial Electronics Society, Lisbon, Portugal, 2019, pp. 4360-4365, doi: 10.1109/IECON.2019.8927006.

[13] A. Credo, M. Villani, M. Popescu and N. Riviere, "Synchronous reluctance motors with asymmetric rotor shapes and epoxy resin for electric vehicles," 2019 IEEE Energy Conversion Congress and Exposition (ECCE), Baltimore, MD, USA, 2019, pp. 4463-4469, doi: 10.1109/ECCE.2019.8912668.